Titre: Title:	Properties of blends of amorphous and semicrystalline \<scp\>PLAs\</scp\> containing multiwalled carbon nanotubes
Auteurs: Authors:	Mojtaba Mohammadi, Mohammadreza Nofar, & Pierre Carreau
Date:	2024
Type:	Article de revue / Article
Référence: Citation:	Mohammadi, M., Nofar, M., & Carreau, P. (2024). Properties of blends of amorphous and semicrystalline \<scp\>PLAs\</scp\> containing multiwalled carbon nanotubes. The Canadian Journal of Chemical Engineering, 25463 (12 pages). https://doi.org/10.1002/cjce.25463

URL de PolyPublie: PolyPublie URL:	https://publications.polymtl.ca/59137/
Version:	Version officielle de l'éditeur / Published version Révisé par les pairs / Refereed
Conditions d'utilisation: Terms of Use:	CC BY-NC-ND

Titre de la revue: Journal Title:	The Canadian Journal of Chemical Engineering
Maison d'édition: Publisher:	Wiley Blackwell
URL officiel: Official URL:	https://doi.org/10.1002/cjce.25463
Mention légale: Legal notice:	This is an open access article under the terms of the Creative Commons Attribution-NonCommercial-NoDerivs License, which permits use and distribution in anymedium, provided the original work is properly cited, the use is non-commercial and no modifications or adaptations are made.© 2024 The Author(s). The Canadian Journal of Chemical Engineering published by Wiley Periodicals LLC on behalf of Canadian Society for Chemical Engineering.

RESEARCH ARTICLE

THE CANADIAN JOURNAL OF
CHEMICAL ENGINEERING

Properties of blends of amorphous and semicrystalline PLAs containing multiwalled carbon nanotubes

Mojtaba Mohammadi[1] | Mohammadreza Nofar[2] | Pierre J. Carreau[1]

[1]Center for High Performance Polymer and Composite systems (CREPEC), Department of Chemical Engineering, Polytechnique Montréal, Montreal, Québec, Canada

[2]Sustainable and Green Plastics Laboratory, Metallurgical and Materials Engineering Department, Faculty of Chemical and Metallurgical Engineering, Istanbul Technical University, Istanbul, Turkey

Correspondence
Pierre J. Carreau, Center for High Performance Polymer and Composite systems (CREPEC), Department of Chemical Engineering, Polytechnique Montréal, Montreal, QC, H3T 1J4, Canada.
Email: pierre.carreau@polymtl.ca

Abstract

Blend nanocomposites of amorphous polylactide (aPLA) and semicrystalline PLA (scPLA)-multiwalled carbon nanotubes (MWCNTs) were prepared by a twin-screw extruder below the melting temperature of the scPLA. The maximum weight percent of MWCNTs in the blends was 0.9 wt.%. The extrudates were either pelletized immediately or after drawing at a drawing ratio of about 10. According to small amplitude oscillatory shear rheological analysis, the rheological properties of the aPLA/scPLA (85/15 wt.%) drawn sample were significantly increased compared to the undrawn samples. With the presence of MWCNTs, more crystallites could develop in the scPLA, and the electrical conductivity of the aPLA/scPLA nanocomposites was reduced due to the encapsulation of MWCNTs within the crystallites of scPLA. Increasing the temperature during compression moulding to 190°C, which is above the melting temperature of the scPLA, effectively removed this obstacle and the electrical conductivity was increased by a factor of up to 10^6 compared to the samples moulded at 150°C.

KEYWORDS
amorphous polylactide (aPLA), electrical properties, multiwalled carbon nanotubes (MWCNTs), PLA blend nanocomposites, rheological properties, semicrystalline PLA (scPLA), thermal properties

1 | INTRODUCTION

Polylactide (PLA) is increasingly recognized as a sustainable substitute for traditional petroleum-based polymers due to its renewable nature and biodegradability.[1] Despite its environmental advantages, its adoption in high-performance sectors is limited by mechanical and thermal constraints such as brittleness, low impact strength, and low thermal stability, which hinder its applications in areas where durability and thermal resistance are essential.[2] In this study, semicrystalline PLA (scPLA) is used as a reinforcing minor phase. Please note that 'scPLA' in this manuscript refers to semicrystalline PLA and not stereocomplex PLA.

Research indicates that the mechanical properties of PLA are affected by its isomeric composition, molecular weight, and temperature.[3,4] The use of block copolymers has been shown to effectively toughen PLA,[5] and studies on its hydrolysis kinetics have shed light on its degradation behaviour.[6] Strategies such as strain-induced

crystallization and thermal pre-annealing have been explored to enhance PLA's properties,[7,8] along with the use of nucleating agents and plasticizers to improve its crystallization behaviour.[9]

Addressing the challenges of enhancing PLA's functional properties has involved physical blending with other polymers, copolymerization, and the addition of fillers and reinforcements.[10–13] These methods have improved the mechanical strength and the thermal stability, but often introduced complexities like compatibility issues and potential compromises to PLA's biodegradability.[14] The development of polymer nanocomposite has focused on achieving a good dispersion with minimal percolation thresholds to optimize properties.[15]

The concept of in-situ self-reinforcement, incorporating scPLA into an amorphous PLA (aPLA) matrix, leads to improved mechanical and thermal characteristics.[3,8] This approach not only serves as a reinforcement mechanism, but also introduces crystallinity to aPLA, potentially leading to improved toughness, stiffness, and thermal resistance. The incorporation of scPLA has resulted in enhanced mechanical strength and thermal properties, evidenced by the effective dispersion of reinforcing agent[11,12] and the use of stereocomplex crystals in PLLA/PDLA expensive blend systems.[16]

In our recent study,[8] a low-cost in-situ self-strengthening method was introduced by inducing fibre-like oriented crystal network of a scPLA within an aPLA through drawing of the extrudate blend processed below the melting temperature of the scPLA. The resulting fibre-like oriented crystal network significantly improved the melt strength and processability of PLA. This enhancement makes the material suitable for various manufacturing methods, including film blowing, fibre spinning, foaming, and injection moulding, which involve stretching and orientation after melt mixing. Building on our previous work,[8] this study focuses on aPLA/scPLA blends enhanced with multiwalled carbon nanotubes (MWCNTs). MWCNTs are chosen for their mechanical strength, thermal conductivity, and electrical conductance.[17,18] The synergy of scPLA and MWCNTs is expected to enhance the aPLA matrix, yielding nanocomposites of superior properties. A twin-screw extruder was employed to prepare the nanocomposites, aiming for a homogeneous dispersion of the MWNCTs. The extrusion and drawing conditions were optimized to induce the formation of fibre-like oriented crystals or crystal clusters in the PLA.[19,20] Comprehensive rheological, thermal, and electrical assessments of the aPLA/scPLA-MWCNT nanocomposites were conducted to understand the complex interactions within the nanocomposite and quantify the improvements in material properties.[21] These analyses highlighted the significant role of MWCNTs in modifying the nanocomposite viscoelastic behaviour and enhancing its thermal and electrical properties.[22–25] The findings of this research are expected to pave the way for the development of high-performance, biodegradable nanocomposites that can meet the requirements of various industrial applications, thereby aligning with the global agenda for sustainability and environmental concerns.

The primary objective of this study is to enhance the performance of PLA blends by incorporating MWCNTs. We aim to improve the rheological, thermal, and electrical properties of the aPLA/scPLA blends. Specifically, the targeted increases in complex viscosity and storage modulus were intended to enhance the material structural integrity, making it suitable for applications requiring durability and high performance. Additionally, the improvement in electrical conductivity, although moderate, aims to meet the requirements for antistatic and electromagnetic interference (EMI) shielding applications. The selected MWCNT content was based on achieving a balance between effective dispersion, property enhancement, and maintaining good processability.

2 | EXPERIMENTAL

2.1 | Materials

Two commercially available PLA grades supplied by NatureWorks LLC (Minnesota, USA) were used in this study: an amorphous PLA grade, Ingeo 10361D (aPLA), with a D-lactic acid content of 12 mol.% and a melt flow rate (MFR) of more than 60 g/10 min at 210°C, served as the matrix; and a semicrystalline PLA grade, 2500HP (scPLA), was used as the reinforcing minor phase, featuring a D-lactic acid content of 0.5 mol.% and MFR values of 8 g/10 min at 210°C. The MFR for the aPLA is reported as 'more than 60 g/10 min' based on the supplier's specifications, indicating its high flowability. The significant discrepancy between the MFR values of aPLA and scPLA is a critical consideration in this study. The high MFR of aPLA provides excellent flowability, aiding in the processing and dispersion of MWCNTs, while the lower MFR of scPLA enhances the structural integrity and mechanical strength of the blend. This combination allows for the optimization of the nanocomposite overall properties, balancing processability and performance. The selection of these two PLA types was based on a fundamental analysis of the dispersion of MWCNTs within matrices of different PLA grades.[4] The MWCNTs were acquired from Cheap Tubes Inc. (Grafton, VT, USA), characterized by an outer diameter of 10–20 nm, an inner diameter of 3–5 nm, a length of 10–30 μm, a specific surface area of 233 m^2/g, and an electrical conductivity greater than 100 S/cm.

2.2 | Melt processing of the nanocomposites

The development of aPLA and scPLA/MWCNTs nano-composites involved a methodically engineered melt processing protocol to augment their rheological and thermal properties. Masterbatches of scPLA with 3 wt.% MWCNTs were first formulated utilizing a twin-screw extruder (Leistritz Advanced Technologies Corp., NJ, USA) equipped with a screw diameter of 18 mm and an *L/D* ratio of 40. The operational parameters were set to a temperature of 190°C and a screw rotational speed of 100 rpm. The extrusion and drawing conditions were optimized to induce the formation of fibre-like oriented crystals or crystal clusters in the PLA matrix. Specifically, the temperature during extrusion was maintained below the melting point of scPLA to preserve its crystalline structure. We employed two methods for pelletizing the extrudates: directly pelletizing the extrudates or drawing them before pelletizing. These methods are crucial for promoting the formation of fibre-like oriented crystals or clusters.

Subsequent to the extrusion, compression moulding of these masterbatches at the same temperature facilitated the preliminary assessment of the rheological behaviour and differential scanning calorimetry (DSC) characteristics.

Prior to blending with the aPLA, the scPLA containing 3 wt.% MWCNTs was subjected to an annealing process in a vacuum oven, set at 90°C for 2 h, to initiate isothermal cold crystallization. This critical preparatory step ensured the scPLA-3CNT had a markedly improved crystallinity, as observed from the results of Figure 1 with an initial crystallinity of 22%–49%.

Post-annealing, aPLA/scPLA blends containing –*x*(wt.%) carbon nanotube (CNT) nanocomposites were prepared (where *x* represents the weight percent of MWCNTs, such as 0.15 or 0.9), adopting a dual strategy to favour a fibrillar network that would bolster the properties of the nanocomposites. The processing of these blend nanocomposites was accomplished using the same twin-screw extruder at a set temperature of 150°C—below the melting point of the scPLA phase—and at the screw speed of 100 rpm. The resulting extrudates were either undrawn (U) and directly pelletized or drawn (D) with a drawing ratio of approximately 10 and at a distance of 2 m from the die exit and the roller prior to pelletizing.

The pellets, whether drawn or undrawn, were put in the vacuum oven overnight at 50°C to eliminate residual moisture. These pellets were then moulded under nitrogen using a hydraulic press at 150°C and compressive force was gradually increased to 29 kN for a period of 10 min to form disk-shaped samples for rheological, DSC, and electrical evaluations. Additionally, for the electrical
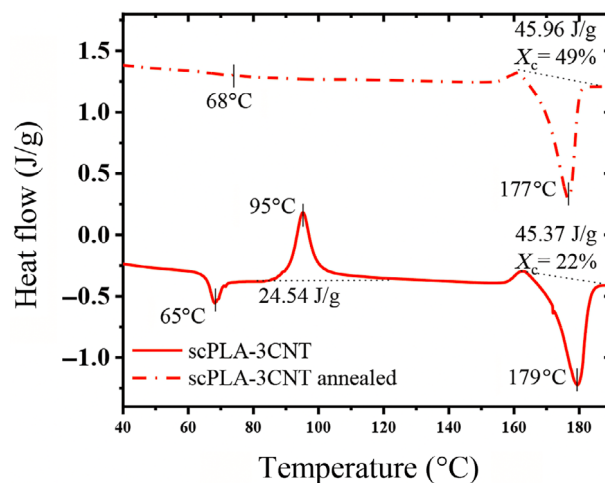
FIGURE 1 Differential scanning calorimetry (DSC) heating thermograms for scPLA-3CNT nanocomposites before and after annealing. The solid line represents the original scPLA-3CNT nanocomposite, which shows a cold crystallization peak at 95°C and a crystallinity of 22%. The dashed line indicates the scPLA-3CNT nanocomposite after annealing, which shows no cold crystallization peak, indicating a significant increase in the degree of crystallinity to 49%. Both compositions have a pronounced melting peak at approximately 177°C. All scanning rates were 10°C/min.

conductivity properties, some samples were prepared at 190°C to investigate the effect of moulding temperature higher than the melting point of scPLA. The quenching effect (directly in cold water) on the electrical conductivity for those samples moulded at 190°C was also investigated.

To provide a clearer understanding of the different processing methods used in this study, we have included a block diagram (Figure 2) illustrating the steps involved in each method.

This comprehensive melt processing approach is tailored to exploit the fibrillation concept, effectively integrating the high aspect ratio of MWCNTs into the aPLA matrix to form an oriented fibre-like crystal network.

3 | CHARACTERIZATION

3.1 | Rheometry

To obtain the viscoelastic properties of the aPLA and scPLA blend nanocomposites, an MCR-302 rotational rheometer (Anton Paar, Austria) was employed within a nitrogen atmosphere, and using a parallel-plate geometry with 25 mm plates, and the gap was set between 1.0 and 1.4 mm. Small amplitude oscillatory shear (SAOS) and stress growth experiments were conducted at 175°C, which is slightly below the melting point of the blend
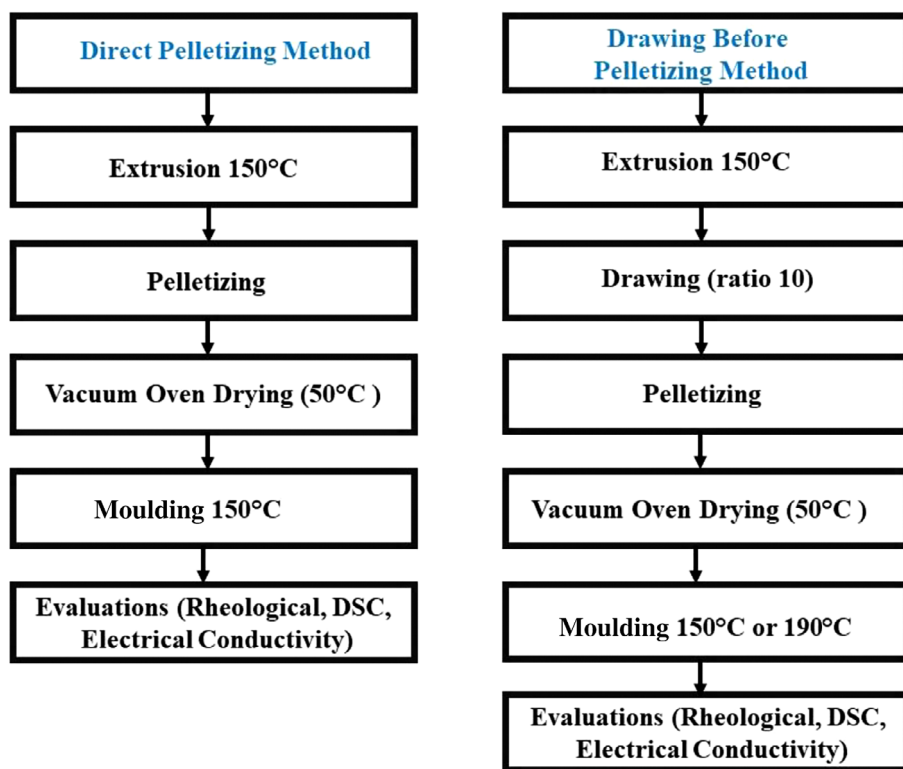
FIGURE 2 Block diagram of the processing approaches used in this study, differentiating between direct pelletizing and drawing before pelletizing.

samples, thus the crystalline structure is preserved during the rheological measurements. The SAOS tests were conducted from high to low frequencies except when mentioned to the contrary. The strain amplitude for the SAOS experiments was set at 0.01 (fractional) to remain within the linear viscoelastic region. It was observed that the rheometer reached temperature equilibrium within 3–4 min before initiating the experiments. Frequency sweeps covered a range from 0.1 to 600 rad/s, taking approximately 17 min to complete. The stress growth experiments were also methodically carried out at 175°C with a shear rate of 0.1 s^{-1} for both undrawn and drawn samples.

It is crucial to note that despite the higher testing temperature, all PLA grades displayed thermal stability during these tests, ensuring that the rheological data are valid within ±10%.

3.2 | Differential scanning calorimetry

The crystallization behaviour of the aPLA/scPLA blends was analyzed using DSC with a Q1000 instrument (TA Instruments, New Castle, DE) under a controlled nitrogen atmosphere to prevent oxidation. The DSC procedure involved heating the samples from ambient temperature up to 200°C with a rate of 10°C/min subsequent to cooling to ambient temperature and second heating to the same value of 200°C with a

rate of 5°C/min and 10°C/min respectively, allowing for a comprehensive investigation into the crystallinity of the blends. This analysis was crucial for understanding the thermal transitions and crystallization kinetics of the aPLA and scPLA composites. The degree of crystallinity, particularly pertaining to the scPLA phase within the blends during the DSC experiments, for non-isothermal behaviour, was quantified using the following equation:

$$X_{\mathrm{h}}(\%) = \left(\frac{\Delta H_{\mathrm{m}} - \Delta H_{\mathrm{cc}}}{93.6}\right) \times 100\% \qquad (1)$$

Equation (1) was used to calculate the total crystallinity of the blend. Here, ΔH_{m} and ΔH_{cc} are the heat enthalpies of melting and cold crystallization, respectively, while α signifies the weight ratio of aPLA in the aPLA/scPLA blends. The constant 93.6 J/g corresponds to the melting enthalpy of completely crystalline PLA, serving as a benchmark for calculating the crystallinity percentage.[26]

3.3 | Electrical conductivity

The electrical resistivity of the samples was assessed by measuring the direct current (DC) resistance across their thickness, which was less than 1 mm. This was achieved

using a Keithley 6517B electrometer/high resistance meter, coupled with a Keithley 8009 resistivity test fixture, both sourced from Keithley Instruments in Cleveland, Ohio, USA. The applied voltage during these measurements was varied between 1 and 100 V, contingent upon the resistivity of the samples. The electrical resistivity (the reciprocal of volume resistivity) readings were recorded following a stabilization period of approximately 60 s. Prior to conducting these measurements, the samples were subjected to drying in an oven the day before and their surfaces were cleansed with ethanol to remove any contaminants.

4 | RESULTS AND DISCUSSION

4.1 | SAOS properties of scPLA/MWCNT nanocomposites

Figure 3 illustrates the small amplitude oscillatory shear (SAOS) rheological properties, namely the complex viscosity (η^*) and storage modulus (G'), as functions of angular frequency (ω) for the neat scPLA and its nanocomposites containing 1 and 3 wt.% MWCNTs. In stark contrast to the neat scPLA, the scPLA nanocomposites with the MWCNT inclusions present a marked departure from the second-order behaviour. The inclusion of 1 wt.% of MWCNTs induces a substantial enhancement in both the complex viscosity (Figure 3A) and storage modulus (Figure 3B), particularly at low frequencies. This increase is by an order of magnitude for the complex viscosity and by four orders of magnitude for the storage modulus, and the behaviour shifts from a liquid to a solid-like material. This effect is further intensified with 3 wt.% MWCNTs, as evidenced by the pronounced rise in the complex viscosity and the emergence of plateaus in the storage modulus at low frequencies. These observations are symptomatic of percolation and a network formation of the multiwalled carbon nanotubes within the scPLA matrix.

4.2 | SAOS properties of aPLA/ (scPLA-3CNT) blend nanocomposites

Figure 4 provides a comprehensive evaluation of rheological properties, namely complex viscosity (η^*) and storage modulus (G'), versus angular frequency (ω) for undrawn (U) and drawn (D) aPLA/scPLA blends, including those drawn (D) with 3 wt.% MWCNTs, representing 0.15 and 0.9 wt.% nanoparticles within the aPLA/scPLA (95/05 wt.%) and aPLA/scPLA (70/30 wt.%) blends, respectively. The measurements were carried out at 175°C, a temperature just below the melting point of the scPLA and the lowest possible, given their significant rigidity at lower temperatures.
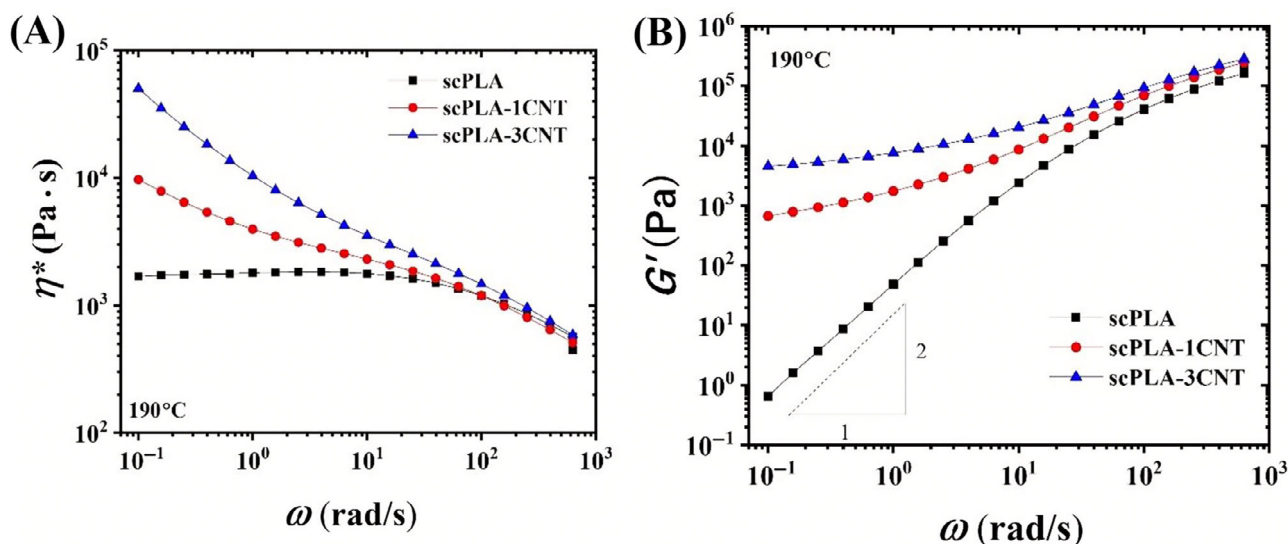
FIGURE 3 Rheological behaviour of semicrystalline PLA (scPLA) and scPLA-carbon nanotube (CNT) nanocomposites at 190°C: (A) Complex viscosity (η^*) as a function of angular frequency (ω) showing the shear-thinning nature of the materials; (B) Storage modulus (G') against angular frequency (ω) highlighting the solid-like behaviour and the influence of multiwalled carbon nanotubes (MWCNTs) concentration on the viscoelastic properties. The neat scPLA (black squares) serves as the baseline, with the red circles representing scPLA with 1 wt.% MWCNTs, and the blue triangles showing scPLA with 3 wt.% MWCNTs. The slight decrease in the complex viscosity of scPLA with decrease in frequency at low frequencies is attributed to thermal degradation of the polymer, which can impact the rheological behaviour.
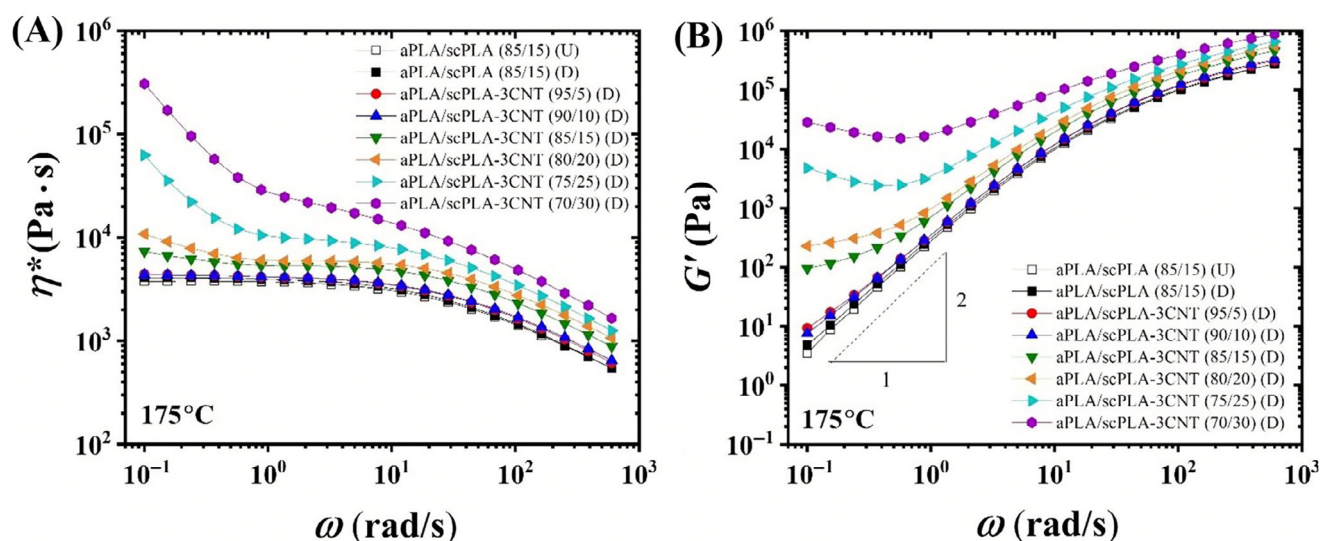
FIGURE 4 Small amplitude oscillatory shear (SAOS) data of amorphous polylactide (aPLA)/semicrystalline PLA (scPLA) blends and their nanocomposites with multiwalled carbon nanotubes (MWCNTs) at 175°C: (A) Complex viscosity (η^*) and (B) storage modulus (G') as functions of angular frequency (ω). Data are shown for undrawn (U) and drawn (D) samples of neat aPLA/scPLA (85/15 wt.%) and aPLA/scPLA with varied weight ratios containing 3 wt.% MWCNTs, equivalent to 0.15–0.9 wt.% MWCNTs in the nanocomposites.

The drawn blend nanocomposites containing 5 and 10 wt.% of the scPLA phase display rheological responses akin to those of the neat aPLA/scPLA (85/15) blend at 175°C. For clarity, only the drawn sets of data are reported. This similarity is confirmed by the characteristic slope of 2 in the low-frequency regime of the storage modulus on the log–log plots of Figure 4B, implying the low effect of the reinforcing fibre-like crystal network on the rheological behaviour. Conversely, the presence of 0.45 wt.% MWCNTs in (aPLA/scPLA-3CNT [85/15]) results in slight enhancements of the complex viscosity and more pronounced increases of the storage modulus, reflecting the combined influence of the fibre-like crystals and MWCNTs.

In samples with higher minor phase contents (20, 25, and 30 wt.%), particularly those subjected to drawing, there are significant upturns in both complex viscosity and storage modulus at low frequencies. This improvement is firstly due to the higher CNT content (that goes from 0.15 for 5 wt.% of scPLA to 0.9% for 30 wt.% scPLA in the nanocomposites). Indeed, the higher CNT content facilitates the development of a percolated network, enhancing the viscoelastic properties. It is also believed to stem from the fibre-like, oriented, and more densely packed crystalline formations for the drawn samples. Indeed, the alignment of scPLA fibres containing higher amounts of CNTs creates an interconnected structure, further contributing to the mechanical reinforcement in the molten state.

Notably, the drawn samples containing 25 and 30 wt.% scPLA exhibit a slight decrease in the storage modulus (G') with increasing frequency at lower frequencies. This initial decline is likely due to cold crystallization occurring during the rheological testing, which affects the viscoelastic behaviour of the material (tests conducted from high to low frequencies). Such behaviour was further explored with sequential SAOS tests, and the findings are reported in Figure 5.

Figure 5 provides a further examination of the influence of cold crystallization on the viscoelastic behaviour of aPLA and aPLA/scPLA-3CNT nanocomposites. The data obtained from tests conducted from low to high frequencies are compared to those obtained from high to low frequencies for the neat aPLA and drawn aPLA/scPLA-3CNT samples with compositions of 75/25 and 70/30 wt.%, against findings from high to low frequency sweeps. For the neat aPLA samples, both sets of data are superposed confirming the polymer thermal stability within the time of the experiments. In contrast, the aPLA/scPLA-3CNT nanocomposites, particularly the drawn samples, display pronounced discrepancies between the low-to-high and high-to-low frequency data. Notably, in the drawn samples, the complex viscosity and storage modulus at low frequencies measured from low to high frequencies are markedly lower compared to those obtained from high to low sweeps. These observations indicate that the time-dependent cold crystallization process significantly impacts the viscoelastic properties of the drawn nanocomposites, probably due to the influence of drawing on cold crystallization. The slightly lower values of the complex viscosity and storage modulus at higher frequencies for tests conducted for low to high frequencies can be attributed to the effect of frequency on cold crystallization.
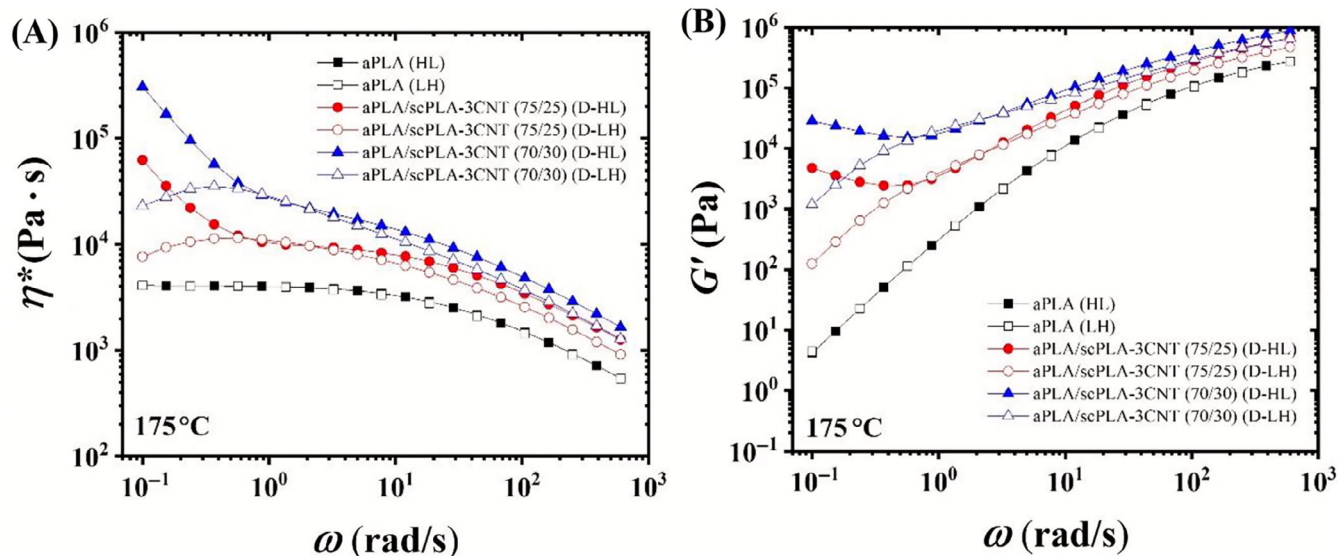
FIGURE 5 Small amplitude oscillatory shear (SAOS) characterization of the neat amorphous polylactide (aPLA) and aPLA/semicrystalline PLA (scPLA)-3carbon nanotube (CNT) nanocomposites at 175°C: (A) Complex viscosity (η^*) and (B) Storage modulus (G') as functions of angular frequency (ω). The data are represented for high to low frequencies (HL) by filled symbols and low to high frequencies (LH) by unfilled symbols) frequency sweeps.

The findings from Figures 4 and 5 elucidate the dynamic nature of crystallization processes in aPLA/scPLA-3CNT nanocomposites and the significant role of drawing on their rheological behaviour. This highlights the complex interplay between material composition, processing history, and thermal treatment, revealing how these factors define the rheological performance of polymer nanocomposites.

Figure 6 reports the complex viscosity (η^*) variations with time for drawn aPLA/scPLA-3CNT samples, highlighting the phenomenon of isothermal cold crystallization at a testing temperature of 175°C. This figure delineates the evolution of η^* for samples containing varying proportions of the minor scPLA phase. Remarkably, distinct upturns in the complex viscosity at low frequencies are evident within the first 2 min for the drawn samples containing the largest ratios of scPLA, confirming the influential role of isothermal cold crystallization. This trend suggests a rapid formation of the reinforcing phase, contributing significantly to the viscoelastic behaviour of the material. The very large variations of the rheological properties with time suggest that the SAOS data reported in Figures 3–5 are not accurate for these samples.

The interplay between the isothermal cold crystallization and the hierarchical structure of the nanocomposites is instrumental in determining the resultant material properties. These findings elucidate that the viscoelastic properties of the drawn aPLA/scPLA-3CNT samples are significantly affected by the presence of MWCNTs and crystallites.
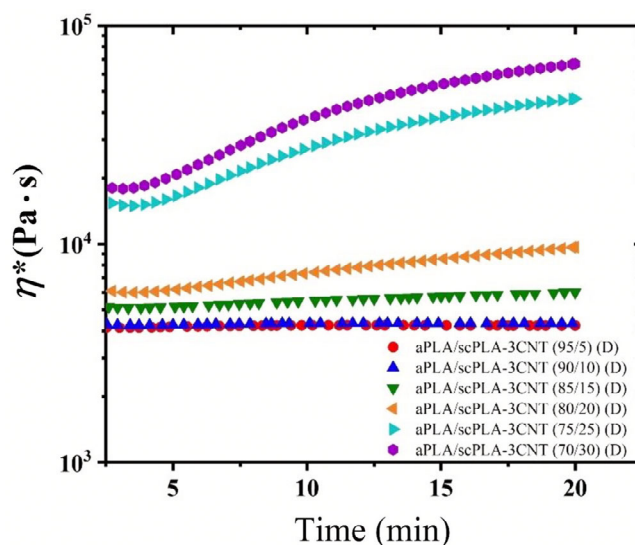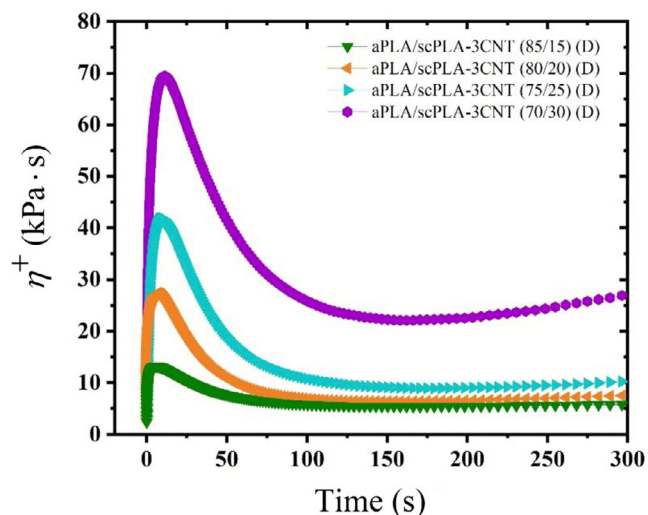

FIGURE 6 Time-dependent variations of the complex viscosity (η^*) for amorphous polylactide (aPLA)/semicrystalline PLA (scPLA)-3carbon nanotube (CNT) drawn (D) nanocomposites across a range of aPLA to scPLA ratios with 3 wt.% multiwalled carbon nanotubes (MWCNTs) at 175°C. The experiments were done at frequency of 1 rad/s and strain of 0.01.
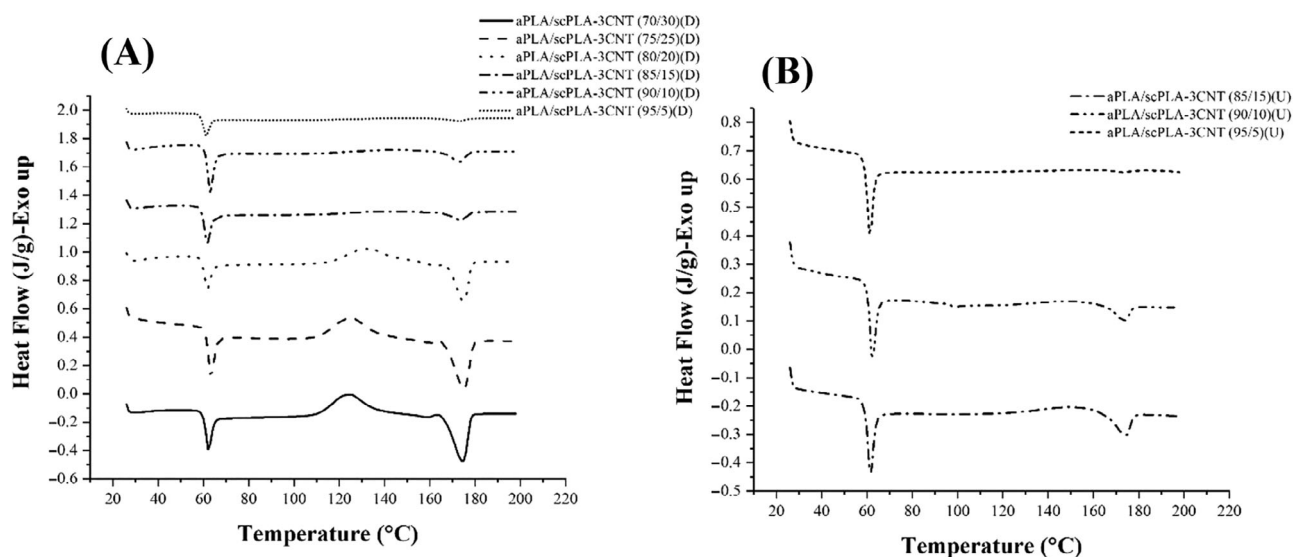
4.3 | Stress growth behaviour

The effects of the fibre-like oriented crystal structures in aPLA/scPLA nanocomposites are substantiated through

stress growth experiments. Figure 7 compares the over-shoots of the transient viscosity of drawn (D) aPLA/scPLA-3CNT blend nanocomposites containing 15–30 wt.% of the minor phase. Conducted at 175°C at an applied shear rate of 0.1 s^{-1} over 20 min, the response is clearly affected by the processing as the drawn nano-composites exhibit very large overshoots of their tran-sient viscosity, confirming the significant role of the isothermal cold crystallization, which is markedly more pronounced for drawn samples due to the contribution

to heterogeneous crystal nucleation. The data for other drawn and undrawn samples are not presented in Figure 7, as no or small overshoots were observed.

4.4 | Thermal properties

Figure 8 provides a comparative analysis of the DSC first heating thermograms for the (A) drawn and (B) undrawn samples. Table 1 summarizes the thermody-namic properties, namely glass transition temperature, heat enthalpy (ΔH_m), degree of crystallinity (X_c), melting temperature (T_m), and cold crystallization temperature (T_{cc}) of these samples.

The DSC measurements presented in Table 1 were performed on disk-shaped samples prepared after mould-ing at 150°C. This temperature was chosen to ensure that the samples were below the melting temperature of semicrystalline PLA, preserving the crystalline structure induced during processing. The absence of a cold cryst-allization peak for the undrawn samples in Figure 8B is due to the specific thermal history and processing conditions. The experimental section clearly indicates that annealing and DSC analysis were conducted at 150°C. Whenever experiments were performed at 190°C for the clarification of crystals and other effects, it was explicitly mentioned in the text.

The tendency observed between undrawn (U) and drawn (D) samples for the lowest amounts of scPLA can be explained by the differences in the degree of orien-tation and crystallinity induced by the drawing process. Drawn samples exhibit higher crystallinity and better

FIGURE 7 Stress growth experiments demonstrating the viscoelastic behaviour and relaxation dynamics of amorphous polylactide (aPLA)/semicrystalline PLA (scPLA)-3carbon nanotube (CNT) nanocomposites; transient viscosity of drawn samples over 300 s at a temperature of 175°C.

FIGURE 8 Differential scanning calorimetry (DSC) first heating thermograms of (A) drawn and (B) undrawn polylactide (PLA) nanocomposites with varying ratios of semicrystalline PLA (scPLA)-3CNT h.

TABLE 1 Summary of DSC heating thermogram results shown in Figure 8.

aPLA/scPLA-3CNT	Glass transition temperature (°C)	Cold crystallization enthalpy (J/g)	Cold crystallization temperature, T_{CC} (°C)	Melting enthalpy, ΔH_m (J/g)	Melting temperature, T_M (°C)	Total degree of crystallinity, X_C (%)
95 wt/5 wt (D)	59	0.3	146	1.1	173	0.9
90 wt/10 wt (D)	59	2.1	146	3.0	174	1.0
85 wt/15 wt (D)	60	1.2	139	2.6	174	1.5
80 wt/20 wt (D)	60	8.1	132	13.1	175	5.3
75 wt/25 wt (D)	61	9.7	125	16.7	176	7.4
70 wt/30 wt (D)	62	10.2	120	17.9	176	8.2
95 wt/5 wt (U)	59	–	–	0.3	173	0.3
90 wt/10 wt (U)	59	1.1	152	2.2	174	1.2
85 wt/15 wt (U)	59	2.2	150	3.5	174	1.3

Abbreviations: aPLA, amorphous polylactide; CNT, carbon nanotube; DSC, differential scanning calorimetry; scPLA, semicrystalline PLA.

alignment of the crystalline regions, which enhances their thermal and mechanical properties. The lower amounts of scPLA may not provide sufficient nucleation sites for a significant crystallization in undrawn samples, leading to the observed differences.

Notably, these samples were processed below the melting temperature of the scPLA, ensuring the retention of the intrinsic crystalline structure of the scPLA phase. The scPLA-3CNT was added to the aPLA as a master-batch, which introduces a dual-phase system: the existing crystalline regions from the scPLA and the induced crystallization induced by the presence of MWCNTs.

Figure 8 and Table 1 reveal that the degree of crystallinity (X_c) in the extruded samples is augmented with the addition of MWCNTs to the aPLA/scPLA blends, that is, by increasing the scPLA-3CNT content, and larger values are obtained for drawn samples except for (90/10 wt.%) sample. A maximum of 8.2% is attained for the aPLA/scPLA-3CNT (70/30 wt.%) (D) sample that contains 0.9 wt.% nanoparticles. The increase in X_c is due to the larger scPLA content and the presence of the MWCNTs, which serve as nucleation agents; cold crystallization is also favoured by the drawing of the extrudate. This assumption is supported by previous studies showing that nanoparticles, including CNTs, facilitate crystallization in polymer matrices.[27–29] Cold crystallization is also favoured by the drawing of the extrudate, which aligns the polymer chains and enhances nucleation. However, we acknowledge that this effect may not be as clear in the three initial formulations for undrawn (U) and drawn (D) nanocomposites, as shown in our DSC results.

The melting temperature (T_m) of the nanocomposite exhibits a slight increase with the increase of the scPLA-3CNT content. This behaviour may be attributed to the combined effect of the preserved crystalline regions of scPLA and the nucleation of new crystallites around MWCNTs, resulting in more stable and possibly larger crystalline regions that necessitate greater thermal energy to melt.[30]

The cold crystallization temperature (T_{cc}) decreases from 146 to 120°C for the drawn blend nanocomposites containing 5% and 30% of minor phase (scPLA-3CNT), respectively, suggesting a reduced energy barrier for crystallization due to the high number of nucleation sites provided by the well dispersed MWCNTs and the pre-existing crystalline regions of the scPLA within the matrix. As a result, the PLA chains are able to organize into a crystalline structure at lower temperatures during the DSC heating cycle. It is worth mentioning that the undrawn (U) samples have higher T_{cc} and the effect of the minor phase contents is not as much as for the drawn (D) samples.

As for the glass transition temperature (T_g), an upward trend is observed with the increment in the scPLA-3CNT content. This phenomenon may be due to the constrained mobility of the PLA chains due to the rigid MWCNT network and the existing scPLA crystallites.[30,31]

4.5 | Electrical conductivity

Among the above prepared samples aPLA/(scPLA-3CNT) (70/30) (D) was selected for analyzing the electrical conductivity as this blend has the largest MWCNT content. For benchmarking purposes, the electrical properties of aPLA/1CNT nanocomposite were also determined.

The nanocomposites were synthesized through a meticulous process using a twin-screw extruder set at 150°C (explained in Section 2.2), a temperature selected to maintain the integrity of the scPLA crystalline structure. Following this, the moulding step was either at

150°C to preserve the crystalline morphology of scPLA or at 190°C to eliminate all crystallites. Furthermore, the effects of rapidly quenching the samples from 190°C directly into cold water was examined.

When moulded at 190°C, the electrical conductivity of the aPLA/(scPLA-3CNT) (70/30) (D) nanocomposites ranged from 10^{-5} to 10^{-6} σ/m (Table 2). The conductivity of this nanocomposite is somewhat lower than that of the aPLA-1CNT sample, which contains more nanoparticles. These values are comparable to conductivities reported previously[4] for similar nanocomposites. This range of electrical conductivity is indicative of the formation of a percolative MWCNT network throughout the PLA matrix. Such a network is characterized by the connectivity of the MWCNTs, forming the conductive pathways through the otherwise resistive PLA environment. This

TABLE 2 Electrical conductivity comparison of aPLA/(scPLA-3CNT) (70/30) (D) composites moulded at different temperatures and the reference aPLA/1CNT composite.

	aPLA/(scPLA-3CNT) (70/30) (D)	aPLA/1CNT
Electrical conductivity for samples moulded at 150°C (σ/m)	~10^{-11}	1.25×10^{-5}
Electrical conductivity for samples moulded at 190°C (σ/m)	10^{-5}–10^{-6}	$2,50 \times 10^{-5}$
Electrical conductivity for samples moulded at 190°C and quenched (σ/m)	5.0×10^{-6}	–

Note: The table presents conductivity values for samples moulded at 150°C, below the melting point of scPLA, and at 190°C, above the melting point, alongside the conductivity after quenching from 190°C.
Abbreviations: aPLA, amorphous polylactide; CNT, carbon nanotube; scPLA, semicrystalline PLA.

behaviour is linked to a degree of crystallinity reduced to 2.0%, as per the DSC analysis (Figure 9A and Table 3; first heating cycle), signifying a structure leaning towards amorphism.

It is observed that the more conductive aPLA/scPLA blend nanocomposites were obtained for samples containing fewer crystals, such as those quenched from 190°C to room temperature(25°C). This observation might seem counterintuitive, as one might expect higher crystallinity to correlate with better conductivity. However, the rapid cooling process during quenching prevents extensive crystallization, resulting in a more amorphous structure. This amorphous structure allows the MWCNTs to remain better dispersed and form a continuous conductive network, thereby enhancing the electrical conductivity. In contrast, higher crystallinity can isolate the MWCNTs within the crystalline regions, disrupting the conductive pathways and reducing overall conductivity. This explains why the quenched samples exhibit higher electrical conductivity despite having lower crystallinity.

In stark contrast, moulding at 150°C, below the melting point of scPLA, leads to dramatic decreases in the conductivity, reaching down 10^{-11} σ/m (Table 2), reflecting an insulating state. This heightened resistivity is attributed to the nanocomposites maintaining a higher degree of crystallinity, recorded at 22.9% (Figure 9A and Table 3; first heating cycle). This crystalline presence is crucial as it implies that post-moulding, the MWCNTs are less able to form extensive networks due to the physical barriers presented by the ordered crystalline domains.

A nuanced DSC analysis provides additional insights into the thermal behaviour of these samples (Figure 9 and Table 3). Specifically, the nanocomposite moulded at 190°C manifested a notable cold crystallization peak with an enthalpy change of 15.8 J/g, succeeded by a melting transition at 13.86 J/g (Figure 9A). This suggests that during the heating cycle, the PLA chains temporarily realign, elevating
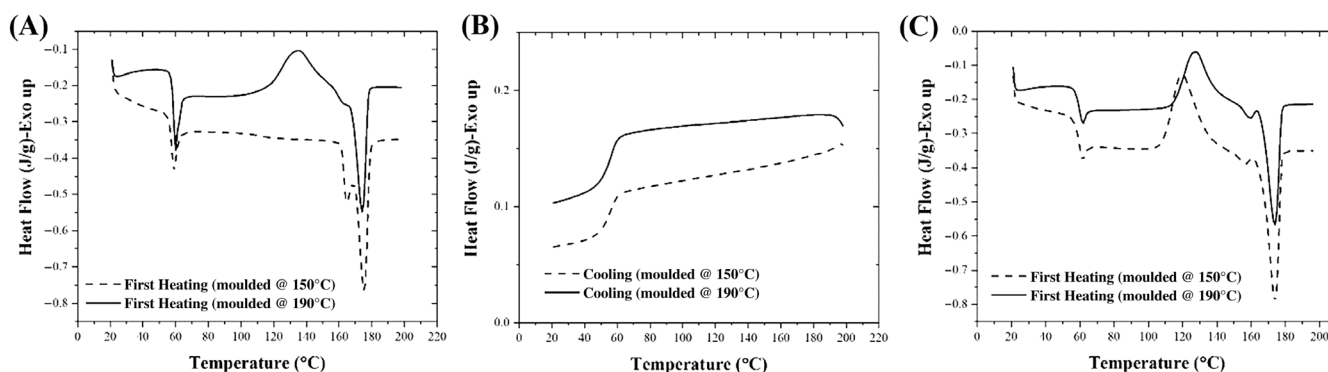
FIGURE 9 Differential scanning calorimetry (DSC) thermograms of amorphous polylactide (aPLA)/semicrystalline PLA (scPLA-3CNT) (70/30) (D) nanocomposites moulded at 150°C (dotted lines) and 190°C (solid lines). (A) first heating cycle; (B) cooling cycle; (C) second heating cycle, all heating and cooling rates are 10 C/min.

TABLE 3 Summary of DSC heating thermogram results shown in Figure 9.

aPLA/ scPLA3-CNT	Cold crystallization enthalpy (J/g)		Cold crystallization temperature (°C)		Melting enthalpy (J/g)		Melting temperature (°C)		Total degree of crystallinity (wt.%)	
	Moulding at 150°C	Moulding at 190°C	Moulding at 150°C	Moulding at 190°C	Moulding at 150°C	Moulding at 190°C	Moulding at 150°C	Moulding at 190°C	Moulding at 150°C	Moulding at 190°C
First heating cycle	–	13.9	–	135	21.4	15.8	175	175	22.9	2.0
Second heating cycle	21.3	13.0	120	127	23.4	18.9	174	174	2.2	6.1

Abbreviations: aPLA, amorphous polylactide; CNT, carbon nanotube; DSC, differential scanning calorimetry; scPLA, semicrystalline PLA.

the crystalline fraction prior to the eventual melting of the crystals. Conversely, the nanocomposite subjected to the lower temperature of 150°C exhibits melting peaks, cumulatively totalling an enthalpy of 21.4 J/g (Table 3). The multiplicity of these peaks may indicate the existence of diverse crystalline fractions within the nanocomposite, corroborating the idea that such fractions are contributing to the overall crystallinity that impedes the conductive network.

The cooling cycle of the nanocomposites did not display any crystallization peaks (Figure 9B), which is a characteristic of the slow crystallization kinetics of the PLA chains. This suggests that the polymer matrix remains largely amorphous during cooling, a factor that could potentially influence the MWCNT dispersion and the subsequent network formation. Upon the second heating cycle (Figure 9C), however, both nanocomposites demonstrate cold crystallization peaks, indicating that the PLA was able to crystallize when reheated. This finding is particularly significant as it reveals the PLA potential for crystallization under appropriate thermal conditions, which does not occur during the initial cooling due to the slow crystallization rate of PLA chains.

The quenching of the nanocomposites from 190°C directly in cold water results in an even larger conductivity of 5.0×10^{-6} σ/m, suggesting a 'locking in' effect of the conductive network by the rapid cooling. This process effectively inhibits the reformation of crystalline domains, thus preserving the connectivity of the MWCNT filler within the matrix (Table 2). These results demonstrate the profound influence of the cooling rates on the conductive properties of polymer nanocomposites, with implications for material design and processing.

Finally, the electrical conductivity values of the aPLA/scPLA blends, though moderate at 10^{-5} S/m, are suitable for antistatic and EMI shielding applications where dissipation of electrical charges is required. The improvement in conductivity by a factor of up to 10^6 under higher processing temperatures demonstrates the potential for tuning processing conditions to achieve higher conductivities. The chosen MWCNT contents (up to 0.9 wt.%) were selected based on achieving a

balance between effective dispersion and significant enhancements in both mechanical and thermal properties, while maintaining overall processability and performance.

5 | CONCLUDING REMARKS

The study on the rheological, thermal, and electrical properties of aPLA and scPLA reinforced with MWCNTs has elucidated the significant enhancements in material performance. The blending of aPLA and scPLA with MWCNTs, followed by a controlled drawing process, has led to the formation of a robust fibrillar network within the polymer matrix, which significantly improved the viscoelastic properties of the blend nanocomposites. The incorporation of MWCNTs not only induced a percolative network that provided structural rigidity but also enhanced the electrical conductivity of the nanocomposites, making them suitable for various high-performance applications.

The thermal analysis revealed that the inclusion of MWCNTs promoted crystallinity in scPLA, which in turn influenced the thermal stability of the nanocomposites. The primary targets for the thermal properties in this study were to achieve higher crystallinity, increase the melting point, and reduce cold crystallization. Higher crystallinity enhances the mechanical strength, thermal stability, and barrier properties of the PLA nanocomposites. Increasing the melting point improves the thermal resistance, allowing the material to maintain structural integrity at elevated temperatures. Reducing cold crystallization temperature and enthalpy enhances the thermal processing window and minimizes undesirable crystallization during processing, indicating a more stable crystalline structure. The electrical studies demonstrated that the conductive pathways formed by MWCNTs are crucial for the enhanced electrical performance of the blend nanocomposites, with the processing conditions playing a pivotal role in defining the conductivity levels. The more conductive aPLA/scPLA blend nanocomposite were

obtained for samples containing less crystals such as quenched from 190°C to room temperature.

AUTHOR CONTRIBUTIONS

Mojtaba Mohammadi: Conceptualization; methodology; validation; investigation; formal analysis; writing – review and editing; writing – original draft. **Mohammadreza Nofar:** Formal analysis; validation; visualization; writing – review and editing. **Pierre J. Carreau:** Formal analysis; resources; funding acquisition; project administration; writing – review and editing; supervision.

PEER REVIEW

The peer review history for this article is available at https://www.webofscience.com/api/gateway/wos/peer-review/10.1002/cjce.25463.

DATA AVAILABILITY STATEMENT

The data that support the findings of this study are available from the corresponding author upon reasonable request.

REFERENCES

[1] J. Rydz, W. Sikorska, M. Kyulavska, D. Christova, *Int. J. Mol. Sci.* **2014**, *16*, 564.

[2] G. Singh, H. Bhunia, A. Rajor, R. N. Jana, V. Choudhary, *J. Appl. Polym. Sci.* **2010**, *118*, 496.

[3] R. Auras, B. Harte, S. Selke, *Macromol. Biosci.* **2004a**, *4*, 835.

[4] M. Mohammadi, Y. Li, J. Randall, M. Nofar, M. C. Heuzey, P. J. Carreau, *Can. J. Chem. Eng.* **2023**, *101*, 5729.

[5] K. S. Anderson, S. Lim, M. A. Hillmyer, *J. Appl. Polym. Sci.* **2003**, *89*, 3757.

[6] S. Lyu, J. Schley, B. Loy, D. J. Lind, C. Hobot, R. Sparer, D. F. Untereker, *Biomacromolecules* **2007**, *8*, 2301.

[7] B. Na, J. Zhu, R. Lv, P. Zhang, Q. Liu, *J. Appl. Polym. Sci.* **2013**, *131*, 1.

[8] M. Nofar, M. Mohammadi, P. J. Carreau, *J. Rheol.* **2021**, *65*, 493.

[9] X. Shi, G. Zhang, T. V. Phuong, A. Lazzeri, *Molecules* **2015**, *20*, 1579.

[10] M. Mohammadi, C. Bruel, M. C. Heuzey, P. J. Carreau, *Cellulose* **2020**, *27*, 9877.

[11] M. Mohammadi, M. Heuzey, P. J. Carreau, *Polym. Compos.* **2021**, *42*, 6688.

[12] M. Mohammadi, M.-C. Heuzey, P. J. Carreau, A. Taguet, *Nanomaterials* **2021**, *11*, 857.

[13] M. Nofar, M. Mohammadi, P. J. Carreau, *J. Appl. Polym. Sci.* **2020**, *137*, 49387.

[14] R. Salehiyan, M. Nofar, K. Malkappa, S. S. Ray, *Polym. Eng. Sci.* **2020**, *60*, 2749.

[15] D. R. Paul, L. M. Robeson, *Polymer* **2008**, *49*, 3187.

[16] P. Purnama, M. Samsuri, I. Iswaldi, *Polymer* **2021**, *13*, 1725.

[17] J. N. Coleman, U. Khan, Y. K. Gun'ko, *Adv. Mater.* **2006**, *18*, 689.

[18] J. Salvetat, G. A. D. Briggs, J. Bonard, R. Bacsa, A. Kulik, T. Stöckli, N. A. Burnham, L. Forró, *Phys. Rev. Lett.* **1999**, *82*, 944.

[19] J. Karger-Kocsis, H. Mahmood, A. Pegoretti, *Prog. Mater. Sci.* **2015**, *73*, 1.

[20] T. Liu, I. Y. Phang, L. Shen, S.-N. Chow, W.-D. Zhang, *Macromolecules* **2004**, *37*, 7214.

[21] F. A. Abdul Azam, Z. Razak, M. K. Fadzly Radzi, N. Muhamad, C. H. Che Haron, A. B. Sulong, *Polymer* **2020**, *12*, 2083.

[22] M. S. Han, Y. K. Lee, W. N. Kim, H. S. Lee, J. Joo, M. Park, H. J. Lee, C. R. Park, *Macromol. Res.* **2009**, *17*, 863.

[23] K. Ke, Y. Wang, K. Zhang, Y. Luo, J. Yang, B. Xie, M.-B. Yang, *J. Appl. Polym. Sci.* **2011**, *125*, E49.

[24] M. Moniruzzaman, K. I. Winey, *Macromolecules* **2006**, *39*, 5194.

[25] D. Wu, Y. Zhang, M. Zhang, W. Yu, *Biomacromolecules* **2009**, *10*, 417.

[26] E. W. Fischer, H. J. Sterzel, G. Wegner, *Kolloid-Zeitschrift & Zeitschrift Für Polymere* **1973**, *251*, 980.

[27] F. Du, R. C. Scogna, W. Zhou, S. Brand, J. E. Fischer, K. I. Winey, *Macromolecules* **2004**, *37*, 9048.

[28] C. Y. Li, L. Li, W. Cai, S. L. Kodjie, K. K. Tenneti, *Adv. Mater.* **2005**, *17*, 1198.

[29] N. Rasana, K. Jayanarayanan, A. Pegoretti, *RSC Adv.* **2018**, *8*, 39127.

[30] M. H. Al-Saleh, *Synth. Met.* **2020**, *265*, 116409.

[31] M. R. R. Hamester, D. F. Pietezak, C. Dalmolin, D. Becker, *J. Appl. Polym. Sci.* **2021**, *138*, 50817.

How to cite this article: M. Mohammadi, M. Nofar, P. J. Carreau, *Can. J. Chem. Eng.* **2024**, 1. https://doi.org/10.1002/cjce.25463